



Measuring Electrocatalytic Activity on a Local Scale with Scanning Differential Electrochemical Mass Spectrometry

K. Jambunathan* and A. C. Hillier**^z

Department of Chemical Engineering, University of Virginia, Charlottesville, Virginia 22903-2442, USA

This paper describes a new technique entitled scanning differential electrochemical mass spectrometry (SDEMS) that combines a quadrupole mass spectrometer with a membrane-covered capillary inlet and a high resolution positioning system that is designed to perform spatial mapping in solution near an electrode interface. Potential applications of this technique include the local characterization of anode catalysts for fuel cells as well as a range of analytical measurements and combinatorial screening studies. The capabilities of this technique are demonstrated by monitoring product evolution in several model electrocatalytic reactions, including the hydrogen evolution reaction, carbon monoxide oxidation, and the direct oxidation of methanol on platinum and platinum-ruthenium electrodes. The inlet of the SDEMS is based upon a small diameter capillary tube to which a nanoporous, hydrophobic membrane is attached. The capillary inlet is positioned near a substrate electrode using a three-dimensional positioning system. The effect of capillary substrate separation and substrate current on the sensitivity and time response of mass spectrometer's ion current are illustrated during hydrogen evolution at a platinum substrate. The sensitivity is demonstrated further by detection of carbon dioxide evolution during the oxidation of a monolayer of carbon monoxide adsorbed on platinum. The ability to address more complex reactions involving complete and partial oxidation products is illustrated with methanol oxidation. In order to demonstrate the ability of this technique to perform spatial mapping, an eight-element band electrode was interrogated for hydrogen evolution and methanol oxidation. Detection of ion currents associated with complete and partial oxidation products of methanol on a set of platinum-ruthenium band electrodes illustrates the ability of this method to spatially discriminate between various reactive sites on a surface, which has potential utility in analytical characterization as well as application as a screening tool in combinatorial catalysis studies.

© 2003 The Electrochemical Society. [DOI: 10.1149/1.1570823] All rights reserved.

Manuscript submitted September 6, 2002; revised manuscript received January 2, 2003. Available electronically April 21, 2003.

The inability of existing anode catalysts in polymer electrolyte membrane fuel cells to oxidize fuels other than hydrogen at sufficient levels has severely limited the development of this technology for practical applications.¹⁻³ Electrode-deactivating species such as carbon monoxide, that are present in fuels either as by-products from upstream reforming or that appear as partial oxidation products during direct oxidation of liquid fuels such as methanol, pose a significant problem for platinum-based catalysts. The strong binding of carbon monoxide to platinum sites leads to catalyst deactivation and decreases reactivity to unsuitable levels.^{4,5} Although improvements in catalytic activity may be achieved over pure platinum by the addition of oxophilic species such as ruthenium,⁶⁻⁹ tin,^{10,11} and molybdenum¹²⁻¹⁴ that promote CO oxidation at lower potentials, necessary levels of performance are yet to be achieved.

One of the barriers impeding the discovery of more active and poison-tolerant anode catalysts is the vast parameter space that must be sampled in order to thoroughly evaluate the ranges of composition and structure that form the basis of the next generation catalysts. The multifunctional requirements of catalysts for the direct oxidation of hydrocarbons, which include the ability to activate C-H, C-O, and even C-C bonds, suggest that optimum performance will require multicomponent binary, ternary, or even quaternary catalysts.¹⁵⁻¹⁷ Combinatorial methods pose great promise to efficiently identify candidate materials or sample vast regions of composition space for further exploration.^{18,19} This was recently demonstrated in a combinatorial study that discovered a new, highly active, four-component anode catalyst for methanol oxidation via an inkjet printer-based array fabrication method combined with an optical screening technique.²⁰

A critical component in the application of combinatorial approaches for catalyst discovery is the development of *in situ*, chemically sensitive screening tools to ascertain reactivity parameters and spatially evaluate catalytic activity.^{21,22} A limited number of screening tools have been developed for catalyst characterization in gas or liquid phases. In gas-phase systems, infrared spectral and thermographic imaging have proven useful for rapid catalyst screening.^{23,24}

Scanning mass spectrometry has also been exploited in both gas and liquid systems.²⁵⁻²⁷ In electrochemical systems, the application of electrode arrays with individually addressable electrodes allows for quantitative measurement of individual reaction currents.²⁸ The ease of constructing microfabricated electrode arrays via traditional microelectronics processing steps has facilitated these studies. Product detection schemes have also been developed. A pH-sensitive optical screening method was employed to identify the onset of methanol oxidation through detection of proton evolution.²⁰ Although this is a rapid and parallel method, it suffers from limited spatial resolution and an inability to discriminate between partial and complete oxidation processes. In addition, quantitative information concerning reaction rates, reaction pathways, and interfacial chemistry is absent in this method. A tactic that is related to the optical screening is to probe the solution environment near an electrode sample using scanning probe techniques. We recently presented a screening method that quantitatively detects the rate of hydrogen oxidation with high spatial resolution using the scanning electrochemical microscope.²⁹ Although this method provides quantitative rate measurements for hydrogen oxidation and can be used to directly probe the generation of protons near a substrate during methanol oxidation,³⁰ the useful pH range of this technique is limited.

In this manuscript, we describe a recently developed technique entitled scanning differential electrochemical mass spectrometry (SDEMS) that functions as a reactivity screening tool and general characterization method for local measurement of dissolved gases and volatile liquid species near electrode surfaces. It consists of a scanning probe microscope that utilizes a mass spectrometer as a detector with a membrane-coated capillary tip as the inlet. This membrane-covered capillary inlet is reminiscent of an earlier paper describing a stationary, membrane-coated pin-hole inlet that was used to indirectly sample single crystal electrodes in a hanging meniscus configuration.³¹ In addition, a recent study describes a scanning mass spectrometry tool that utilizes a membrane-free, scanning capillary tube with a thermospray inlet to completely vaporize a continuously pumped electrolyte sample and detect dissolved solution species.³² Our device has a different sampling scheme that is based upon modification of the differential electrochemical mass spectrometer (DEMS). This technique is based upon the original membrane-inlet, electrochemical mass spectrometry (EMS) design

* Electrochemical Society Student Member.

** Electrochemical Society Active Member.

^z E-mail: ach3p@virginia.edu

of Grambow and Bruckenstein,³³ which was later modified by Wolter and Heitbaum to achieve a faster response time via differential pumping of the inlet.³⁴

A variety of modifications and upgrades to the original DEMS design have been made to expand the capabilities and application of this technique.³⁵⁻³⁸ DEMS has proven a highly valuable method for direct, quantitative measurement of dissolved gases and volatile liquid species present at the electrode-electrolyte interface.³⁹ The ability of DEMS to measure complete and partial oxidation products associated with the oxidation of fuels such as methanol,⁴⁰ formic acid,⁴¹ and ethanol^{35,42} is a particularly appealing feature in the characterization of anode catalysts. DEMS can provide quantitative evidence of product distribution and reaction pathways.^{40,43,44} Identification of the nature of decomposition products and dominant surface bound species⁴⁵⁻⁴⁷ has also been demonstrated through careful product analysis as well as by the application of isotopic reagents.⁴⁸

In this work, the capabilities of SDEMS are demonstrated for several model electrocatalytic reactions, including hydrogen evolution, carbon monoxide oxidation, and the direct oxidation of methanol. General system characteristics as well as time response and sensitivity are illustrated using hydrogen evolution at a platinum substrate. The ability to detect monolayer quantities of product following carbon monoxide oxidation in addition to visualizing complete and partial oxidation products of methanol oxidation are illustrated. The screening capabilities of SDEMS are demonstrated by mapping product evolution at an eight-element band electrode containing electrodeposited platinum-ruthenium catalysts of variable composition.

Experimental

Reagents.—All experiments were performed using electrolytes dissolved in 18 M Ω deionized (DI) water (E-Pure, Barnstead, Dubuque, IA). The solutions were deaerated with nitrogen (BOC Gases, Murray Hill, NJ) prior to measurement. Carbon monoxide studies were achieved by delivering pure CO gas (BOC Gases, Murray Hill, NJ) to the electrochemical apparatus by bubbling through a porous ceramic frit (Ace Glass, Inc., Vineland, NJ) into the electrolyte solution for a period of 5 min with the working electrode held under potential control. The CO was then removed from solution by purging with nitrogen. Electrochemical measurements were performed in solutions containing as-received sulfuric acid (H₂SO₄), sodium sulfate (Na₂SO₄), and methanol (CH₃OH, 99.9%) (Aldrich, Milwaukee, WI). Electrodeposits of Pt and Ru were obtained from solutions containing chloroplatinic acid (H₂PtCl₆) and ruthenium chloride (RuCl₃) (Strem Chemicals, Newburyport, MA).

Electrodes.—Two types of working electrodes were used that included a 2 mm diam polycrystalline Pt disc electrode (Bioanalytical Systems, West Lafayette, IN) encased in poly ether ether ketone (PEEK) and an eight-element band electrode coated on a frosted glass slide (Erie Scientific Company, Portsmouth, NH). Preparation of the Pt disc electrode consisted of polishing with successively finer grades of energy paper to achieve a planar surface, followed by diamond polishing paste and alumina slurry down to 0.05 μ m particle size to produce electrodes that exhibited a mirror finish. The band electrodes were created by metal evaporation through a patterned, aluminum mask containing 8 slits (1 mm width and 2.5 mm period). A coating of 10 nm Ti followed by 100 nm Au (Ernest F. Fullam, Inc., Latham, NY) was evaporated onto the glass slide through the mask using a thermal evaporator (Bench Top Turbo III high vacuum evaporator, Denton Vacuum, LLC, Moorestown, NJ). Pt was then electrodeposited onto these Au bands from a solution containing 5 mM H₂PtCl₆ and 0.1 M Na₂SO₄ at a constant potential of 50 mV (vs. reversible hydrogen electrode, RHE) for 5 min using a eight channel multielectrode potentiostat (model CH1030, CH Instruments, Inc. Austin, TX). Platinum-ruthenium electrodes were electrodeposited from 0.1 M Na₂SO₄ solutions neutralized to pH 7 with NaOH containing different amounts of H₂PtCl₆ and RuCl₃ at a total metal content of 10 mM. Electrodeposition was achieved by

applying a potential pulse program between -0.15 and -1.57 V vs. Hg/Hg₂SO₄ at a frequency of 100 Hz via a potentiostat (model 283, EG&G Instruments, Oak Ridge, TN) using a function generator (Global Specialties, New Haven, CT). The various band electrodes were created serially starting with a pure Ru band followed by bands with increasing Pt content. An individual band was coated with a Pt_xRu_y electrodeposit and then the solution was removed. The cell was then rinsed with DI water and a new Pt/Ru solution was injected for the next band. Creating the pure Pt electrode last was necessary to avoid exposing the Pt electrode to RuCl₃ solution and, thus, preventing the spontaneous deposition of Ru on the Pt electrode.^{49,50} However, the spontaneous deposition of Pt on Ru can also occur, but the data for our samples suggested that this process did not occur to a significant degree.^{51,52} The electrode compositions were verified using both Auger electron spectroscopy (AES) and energy dispersive spectroscopy (EDS), which gave identical composition measurements within measurement error.

Before use, the working electrodes were sonicated in an ethanol/water solution and then rinsed with copious amounts of DI water. Further electrode pretreatment included electrochemical potential cycling between water oxidation and hydrogen evolution in an aqueous solution of 0.5 M H₂SO₄ until a characteristic voltammetric signature of a polycrystalline platinum surface was obtained. This electrochemical treatment was not performed for the Pt_xRu_y electrodes to avoid the oxidative dissolution of Ru that occurs at positive potentials. A length of Pt_{0.8}Ir_{0.2} wire (Goodfellow Corporation, Berwyn, PA) was used as a counter electrode. The reference electrode consisted of a AgCl-coated Ag wire. The potential scale of this electrode was verified against a standard calomel electrode and converted to the RHE scale. All data are presented vs. the RHE.

Two types of electrochemical cells were used. For experiments performed with the Pt disc electrode, the electrochemical cell was made from Teflon with a cell volume of 100 mL. The cell contained slots for reference, counter, and working electrodes. The working electrode was positioned in a slot at the bottom of the cell with a vertical orientation and the electrode surface facing up. The cell was made leak-proof by pressure fitting all electrodes with Teflon tape. The cell also contained a slot for a right angle glass prism (Edmond Scientific, Barrington, NJ), which was used to visualize the gap between capillary tip and working electrode. For experiments performed with the band electrodes, a 1 \times 0.5 in. rectangular glass tube (Whale Apparatus Company, Inc., Hellertown, PA) was glued directly to the band electrode assembly using an insulating lacquer (WB-018 Stop-Off Coating, Michigan Chrome & Chemical Company, Hope, AK). The eight working electrodes were connected to a twenty pin dip-clip (Pomona Electronics, Pomona, CA) to allow potential control of individual electrodes or the entire assembly.

SDEMS.—The SDEMS used here consisted of an electrochemical cell and potentiostat combined with a mass spectrometer and three-dimensional (3-D) positioning system, which were all under computer control (Fig. 1). The mass spectrometer (MS) was a QMS 200 (Pfeiffer Vacuum, Nashua, NH) consisting of a quadrupole mass analyzer using a Channeltron detector with mass resolution of $m/z = 0.5$ atomic mass units (amu) and a mass range up to 200 amu. The spectrometer utilized an electron impact (EI) ionization source. Pumping of the detector's ionization chamber was achieved with a combination of mechanical diaphragm roughing pump and a turbomolecular pump, which were capable of an ultimate pressure approaching 10^{-7} Torr. The inlet to the MS consisted of a sampling probe that was a 10 cm long, 150 μ m inner diam (i.d.) poly(tetrafluoroethylene) (PTFE) capillary tube (Valco Instruments, Houston, TX) to which a 20 nm pore size Gore-Tex membrane was secured with shrink tubing. This capillary was connected to a T-connector fitting (Valco Instruments, Houston, TX) that was further connected to the mass spectrometer ionization chamber with a 10 cm, 1 mm diam stainless steel (SS) rod and a rotary vane pump

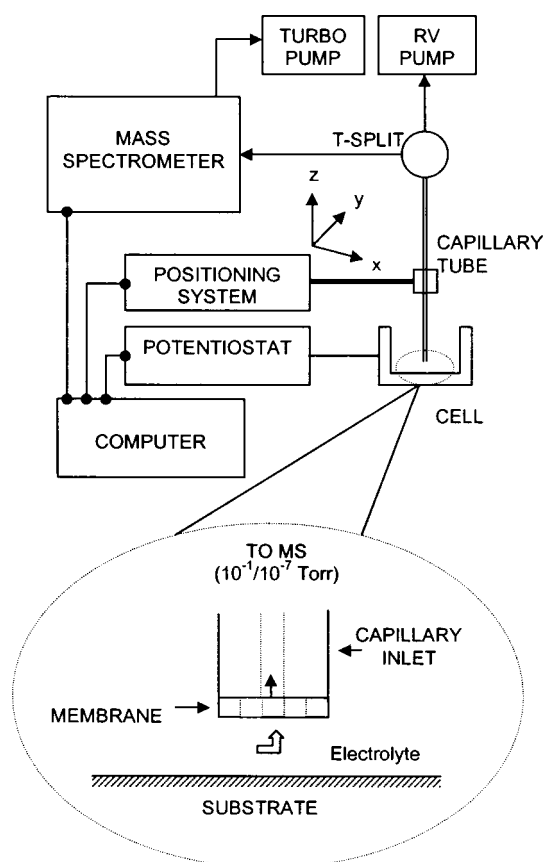


Figure 1. Schematic of SDEMS showing major system components. Inset depicts magnified view of tip/sample interface and capillary/membrane inlet.

(RV5, BOC, Edwards, Wilmington, MA) to provide differential pumping of the inlet. The rotary vane pump provided an ultimate vacuum of 0.1 Torr within the T connector.

The capillary sampling probe was mounted to a holder attached to three piezoelectric inchworm motors (model IW-710, Burleigh Instruments, Inc., Fishers, NY). The motors were mounted directly onto one TS-300 (z) and two TS-100 (xy) translation stages configured for 3-D orthogonal motion. The complete assembly was mounted directly to an optical breadboard (Newport Corporation, Irvine, CA). The inchworm motors had a 25 mm range of motion, a mechanical resolution of 4 nm, and optical encoders giving an absolute position reproducibility of 0.5 μm . Position control of the capillary inlet was achieved with a Series 6200 ULN Controller (Burleigh Instruments, Inc., Fishers, NY). Electrochemical measurements were performed using a bipotentiostat (AFDRE, Pine Instrument Company, Grove City, PA). Data collection was achieved using a commercial mass spectrometer controller program (Quadstar, Balzers Limited, FL) with additional analog input channels to allow synchronization of the electrochemical signals (substrate current and potential) with up to 64 additional mass channels.

Results and Discussion

The configuration of the SDEMS is depicted in Fig. 1. The key components included an electrochemical cell with a substrate electrode connected to a potentiostat, a high resolution micropositioning system, a quadrupole mass spectrometer with a differentially pumped, capillary inlet and a computer for data acquisition and control (Fig. 1). The inlet to the spectrometer comprised a capillary tube with an i.d. of 150 μm . The entrance of this capillary tube was covered with a nanoporous, hydrophobic membrane. The small inlet diameter increased the spatial resolution and the hydrophobic membrane coating separated the liquid electrolyte from the high vacuum

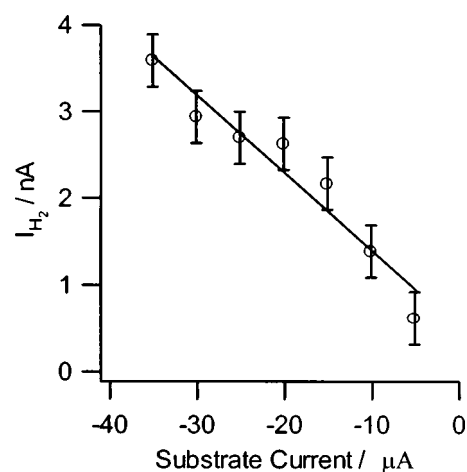


Figure 2. Amplitude of hydrogen ion current (I_{H_2} , $m/z = 2$) as a function of substrate current at a capillary/substrate separation of approximately 100 μm . Solution: deaerated 0.5 M H_2SO_4 .

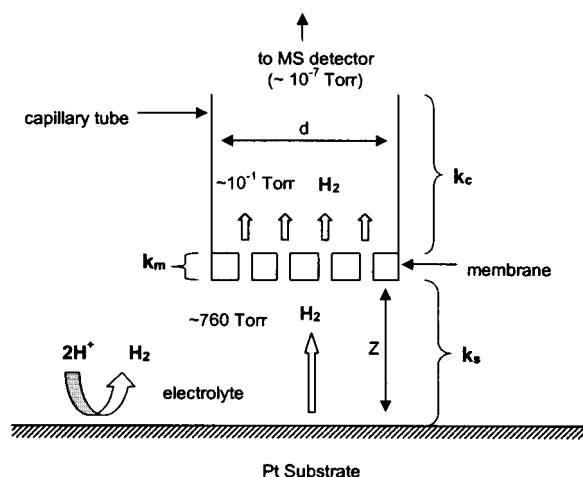
conditions existing within the ionization chamber of the mass spectrometer. The hydrophobic nature of the membrane coating is critical to the operation of this detector and in particular served to reduce the quantity of water within the spectrometer. The position of the capillary inlet was controlled with high precision using a computer-controlled, 3-D positioning stage. For measurements that involve detecting species evolved from a specific location on a substrate electrode, the tip-substrate gap was reduced to the smallest possible value of typically less than 100 μm in order to maximize the collection of surface generated species and minimize the time delay between the evolution of a species at the electrode surface and its detection in the spectrometer.

Hydrogen evolution and SDEMS characteristics.—The ability of the MS to detect dissolved gases or other volatile species when immersed in an aqueous solution is key to using this method for the characterization of electrochemical processes. A model reaction that illustrates the various features and capabilities of this technique is the hydrogen evolution reaction (HER)



where the hydrogen that is evolved at a substrate electrode can be monitored with the MS. In order to verify the differential mode of detection and to provide an illustration of the sensitivity, steady-state ion current values were monitored as a function of the substrate current during hydrogen evolution. Figure 2 shows the steady-state ion current values for $m/z = 2$ at a tip-substrate separation of $\sim 100 \mu\text{m}$ for several substrate current values between -5 and $-35 \mu\text{A}$. Although there is some scatter in the data, a near-linear relationship between the ion current and substrate current is observed. This is the expected response for a DEMS configuration and indicates that the tip response is proportional to the flux of hydrogen evolving from the substrate surface. Thus, the spectrometer is detecting the differential response as is typical for DEMS.³⁴ In addition, the current sensitivity at the smallest tip-substrate gap is approximately 1 nA per 10 μA of substrate current at a 0.03 cm^2 electrode. This gives an area-normalized sensitivity of 3×10^{-6} nA (hydrogen ion current)/nA cm^{-2} (substrate current).

In order for a species like hydrogen that is produced at the electrode surface to be detected by the mass spectrometer, it must diffuse from the substrate to the membrane inlet, pass through the length of the capillary tube into the ionization chamber. The ion current (I_i) for any species i will be related to its flux (N_i) into the ionization chamber times the capillary area (A_c) and a calibration constant (Λ_i) according to



Scheme 1. Schematic of mass spectrometer inlet in electrolyte solution during hydrogen generation at a platinum substrate. Mass transfer coefficients are shown corresponding to the electrolyte solution (k_s), membrane film (k_m), and capillary tube (k_c) regions.

$$I_i = \Lambda_i N_i A_c = \Lambda_i K_i \Delta p_i A_c \quad [2]$$

where Δp_i is the pressure difference for species i between the substrate electrode and in the ionization chamber and K_i is an overall mass transfer coefficient. The flux can be described with a simple model that considers three mass transfer steps occurring in series (Scheme 1). The individual steps include diffusion from the substrate through solution to the membrane ($k_{s,i}$), transport across the membrane ($k_{m,i}$), and convection down the capillary tube to the ionization chamber ($k_{c,i}$). The overall mass transfer coefficient can be written as a combination of the three individual mass transfer coefficients according to

$$1/K_i = 1/k_{s,i} + 1/k_{m,i} + 1/k_{c,i} \quad [3]$$

where the overall process can be influenced by all three steps or dominated by one or two. Ultimately, the sensitivity and time response of the SDEMS can be optimized by increasing the rates of all mass transfer steps.

Steady-state mass transfer from the substrate to the membrane can be approximated by diffusion through a thin gap

$$k_{s,i} = \frac{D_i}{H_i Z} \quad [4]$$

where D_i is the diffusion coefficient of species i in solution, Z is the membrane/substrate gap distance, and H_i is the Henry's law constant for species i . Thus, the diffusion coefficient of each species in solution impacts upon the intensity as well as the time response of the ion signal. A smaller diffusion coefficient will reduce the measured mass intensity and create a slower time response for that species. A decrease in the Henry's law constant, which is equivalent to an increase in gas solubility in the liquid phase, will serve to increase $k_{s,i}$. Therefore, highly soluble gas species will exhibit a higher $k_{s,i}$ value. Ultimately, reducing the influence of mass transfer in the solution phase for all species can most effectively be achieved by decreasing the membrane/substrate gap distance Z to the smallest possible values.

Mass transfer across the membrane is best estimated by Knudsen diffusion through a small, gas-filled pore

$$k_{m,i} = \frac{\varepsilon D_i^{\text{Kn}}}{RTL_m} \quad [5]$$

where ε is the membrane void fraction representing the open pore area, D_i^{Kn} is the Knudsen diffusion coefficient for species i , L_m is the membrane thickness, T is the temperature, and R is the gas constant. The Knudsen diffusion coefficient can be estimated from the kinetic theory of gases according to

$$D_i^{\text{Kn}} = \frac{d}{3} \left[\frac{2RT}{M_i} \right]^{1/2} \quad [6]$$

where d is the pore diameter and M_i is the molecular weight of species i .⁵³ This equation indicates that species will diffuse through the membrane at different rates that are determined by differences in their molecular weights. However, control experiments (*vide infra*) suggest that the membrane does not present a substantial mass transfer barrier for the diffusion of gases and, thus, fractionation at this interface is limited.

The final mass transfer step involves transporting species from the inner membrane surface down the capillary tube into the ionization chamber of the mass spectrometer. This process can be best described as viscous flow where the gas velocity is pressure-driven and obeys the Hagen-Poiseuille law.⁵³ The corresponding mass transfer coefficient for this process has the form

$$k_{c,i} = \frac{d^2 \Delta p}{32 \mu L_c} \quad [7]$$

where Δp is the total pressure difference between the membrane surface and the ionization chamber, μ is the gas viscosity, and L_c is the length of the capillary tube. Clearly, this mass transfer process is independent of the species involved and is simply a function of the pressure drop and the capillary dimensions. This process can be accelerated by increasing the capillary diameter, increasing the pressure drop, or by decreasing the capillary length.

The controlling mass transfer process in this system was evaluated by comparing the response in liquid to that in laboratory air with and without the membrane. The rate of mass transfer down the length of the capillary was estimated by measuring the time response of the detector to gas dosing in laboratory air in the absence of the membrane. Following exposure of the capillary inlet to carbon dioxide, an almost instantaneous increase in ion current was observed for $m/z = 44$. The time constant for this response was estimated at less than 1 s. This indicated that the value of the mass transfer coefficient ($k_{c,i}$) down the capillary tube was quite large. A similar experiment was performed in laboratory air with a membrane-coated capillary inlet. The time response was again almost instantaneous, indicating a large value for the mass transfer coefficient through the membrane ($k_{m,i}$). Thus, the membrane does not present a substantial mass transfer limitation for the diffusion of gases.

The time response of the system in solution was then evaluated for the series of transient curves measured during hydrogen evolution at a substrate electrode. Figure 3 depicts measurement of the hydrogen ion current ($m/z = 2$) with the capillary inlet positioned near a polycrystalline Pt disk electrode. The electrochemical substrate current is stepped from zero to a constant value of $-20 \mu\text{A}$ while the ion current in the MS is monitored. Under these conditions, protons are reduced at the substrate and hydrogen is evolved at a constant rate. The MS ion current is plotted as a function of time at separations of 60, 210, and 500 μm between the capillary inlet and substrate electrode.^a The shapes of the transient curves exhibited

^a The absolute separation between tip and substrate is determined in these measurements by visual inspection using a charge-coupled device camera fit with a variable, zoom lens. The intrinsic error in this measurement derives from the difficulty in determining absolute tip-substrate contact.

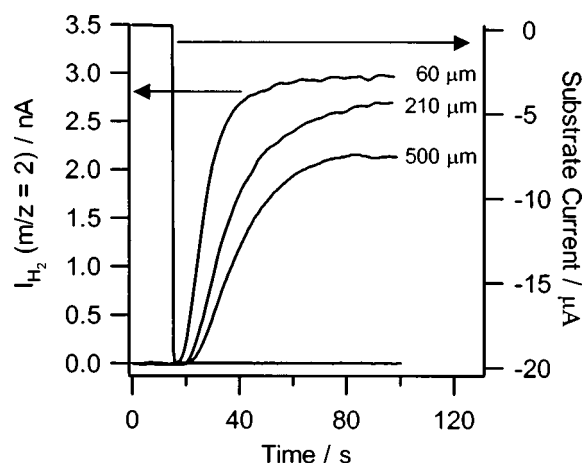


Figure 3. Plot of hydrogen ion current ($I_{\text{H}_2, m/z = 2}$) evolving from a Pt substrate electrode following a current step ($0 \mu\text{A}$ to $-20 \mu\text{A}$) at capillary/substrate separations of 60, 210, and 500 μm . Solution: deaerated 0.5 M H_2SO_4 .

a characteristic response, where the hydrogen ion current (I) can be represented by a first-order with dead-time model.⁵⁴

$$I = 0 \quad t < \theta_d$$

$$I = A \left[1 - \exp\left(-\frac{(t - \theta_d)}{\tau}\right) \right] \quad t > \theta_d \quad [8]$$

As the tip/substrate separation is decreased from a gap distance of 500 to 60 μm , the amplitude (A) of the measured ion current increases while the magnitude of both the dead time (θ_d) and time-constant (τ) decrease. The increase in ion current reflects an increase in amount of sampled hydrogen, which is equivalent to an increase in the collection efficiency, as the tip is positioned closer to the substrate surface. The decrease in time constant and dead time are a reflection of the increased speed at which products generated at the substrate electrode reach the capillary tip with decreasing gap distance.

The series of transient, galvanostatic measurements depicted in Fig. 3 were fit to the first-order model (Eq. 8) and the results are summarized in Fig. 4. Figure 4A depicts the steady-state ion current measured at a tip/substrate separation ranging from 0 up to 1200 μm for a fixed substrate current of $-20 \mu\text{A}$. Each data point represents the mass spectrometer ion current for hydrogen ($m/z = 2$) measured 2 min following a step in the substrate current and, therefore, reflects the steady-state hydrogen generation rate. The response shows an increasing ion current as the tip/substrate separation is decreased that follows a linear trend. This behavior indicates that the efficiency of tip collection improves with decreasing tip/substrate separation. The tip is able to capture a greater fraction of the substrate-generated hydrogen as it is positioned closer to the source of the hydrogen. In Fig. 4A, the steady-state current levels off at a separation of approximately 200 μm and does not increase at smaller separations. This is likely a result of the tip and substrate making contact at this separation. In the present configuration, the capillary tube used for the tip has an i.d. of 150 μm but an outer diam (o.d.) of approximately 1.5 mm, which makes reducing the tip/substrate separation to very small values difficult. It is expected that improvements to this response may be achieved by constructing smaller or conical tips, whose physical dimensions have been reduced to limit unwanted tip/substrate contact.

The values for the time constant and dead time are plotted in Fig. 4B at various separations. Both parameters decrease in magnitude with decreasing tip/substrate separation. The time constant exhibits a value of nearly 70 s at a separation of 1200 μm and approaches 10 s at a separation of less than 200 μm . The dead time varies from a

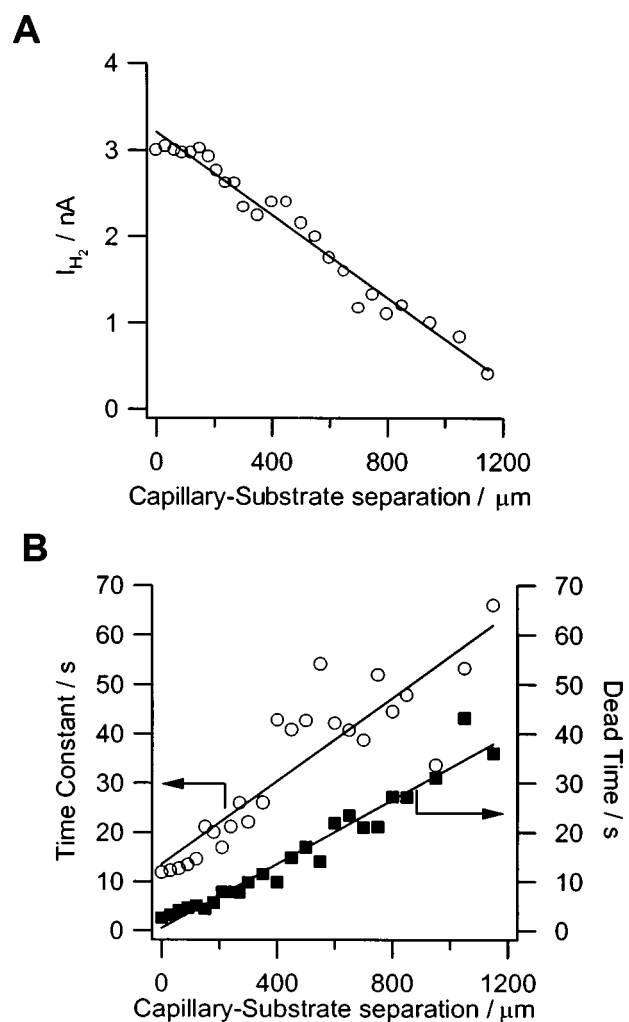


Figure 4. (A) Plot of hydrogen ion current ($I_{\text{H}_2, m/z = 2}$) as a function of capillary/substrate separation at a substrate current of $-20 \mu\text{A}$. (B) Open circles show plot of time constant and filled squares show dead time corresponding to fits of current-step experiments for hydrogen evolution as a function of capillary/substrate separation. Solution: deaerated 0.5 M H_2SO_4 .

high of 40 s to a low of almost 0 s over this separation range. This behavior can only be explained by mass transfer that is controlled by the liquid phase where the value for $k_{s,i}$ is much smaller than $k_{m,i}$ and $k_{c,i}$. Clearly, decreasing the tip/substrate separation increased the value of $k_{s,i}$. With the current experimental assembly, the fastest time response that could be achieved indicated a time constant between 2 and 10 s with the tip immersed in liquid. Under these conditions, it was estimated that over 90% of the resistance to mass transfer is in the liquid phase. Improvements to this response may be achieved by developing smaller tips that can be positioned closer to the substrate surface without contact.

Carbon monoxide oxidation.—A variety of species in addition to hydrogen can be detected with this SDEMS system just as has been previously demonstrated with traditional DEMS.^{39,41,55} Of particular interest are reagents relevant to anode reactants in fuel cells. DEMS has been used to monitor the oxidation of various hydrocarbons, including carbon monoxide, formic acid, methanol, ethanol, and a variety of other potential fuels. Complete oxidation can be directly measured by monitoring the evolution of carbon dioxide and a quantitative analysis provides a measure of the system's current efficiency.⁴⁰ An example of CO_2 detection is illustrated in Fig. 5. In this experiment, a monolayer of CO is adsorbed onto the sur-

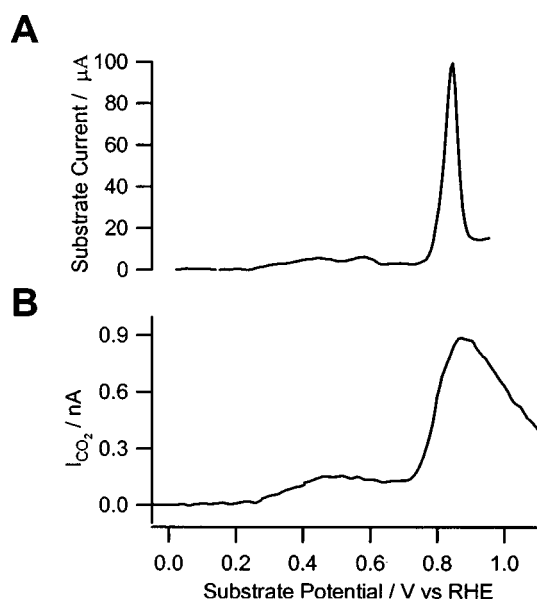


Figure 5. Electrochemical and mass spectrometric response of Pt substrate during oxidation of a CO monolayer in a nitrogen-purged solution containing 0.5 M H₂SO₄ at a scan rate of 10 mV s⁻¹. (A) Electrochemical current and (B) CO₂ ion current ($I_{\text{CO}_2}, m/z = 44$).

face of a polycrystalline Pt electrode. This was achieved by exposing that surface to aqueous electrolyte saturated with dissolved CO for a period of 5 min while holding the electrode potential at 0.1 V (vs. RHE). The solution is then purged with nitrogen. Subsequently, the adsorbed CO layer is oxidized to CO₂ by scanning the substrate electrode in the positive direction. The capillary inlet tip is positioned near the electrode surface, and the substrate current and CO₂ ion current ($m/z = 44$) are monitored.

The electrochemical current observed in Fig. 5A is typical of CO monolayer oxidation from polycrystalline Pt.^{4,5} A high coverage CO layer forms following adsorption at substrate potentials in the hydrogen under potential deposition (UPD) region. Scanning the electrode potential in the positive direction results in a prewave starting just positive of 0.2 and extending up to 0.6 V. This prewave is associated with oxidation of “weakly bound” CO via adsorbed water and amounts to a loss of ~0.1 monolayer.^{4,5,56,57} The simultaneously measured CO₂ ion current exhibits an increase in magnitude at potentials in the prewave region. Thus, the MS is detecting CO₂ that evolves from the surface during oxidation of the weakly bound CO. Clearly, the detector is sensitive to submonolayer quantities of CO₂. Further positive excursions in the substrate potential produce the main oxidation wave with a peak centered at 0.8 V. The remainder of the CO layer is oxidized to CO₂ during this process. The CO₂ ion current signal responds to the main oxidation peak by increasing in accordance with the formation of additional CO oxidation product. Notably, a tail is observed in the ion current signal at positive potentials that is absent in the electrochemical current. This tail is related to the time required for CO₂ generated at the substrate to diffuse to the capillary inlet. The magnitude of this diffusional tailing decreases at slower potential scan rates.

Methanol oxidation.—The ability to simultaneously detect several species associated with an electro-oxidation reaction is illustrated by the oxidation of methanol on a Pt electrode (Fig. 6). The electrochemical current depicts the characteristic behavior of methanol oxidation on Pt under acidic conditions. The hydrogen UPD current is suppressed at low potentials due to the formation of strongly bound, electrode-deactivating species that are produced from methanol decomposition at the electrode surface.^{58,59} The substrate current maintains a low value as the electrode potential is

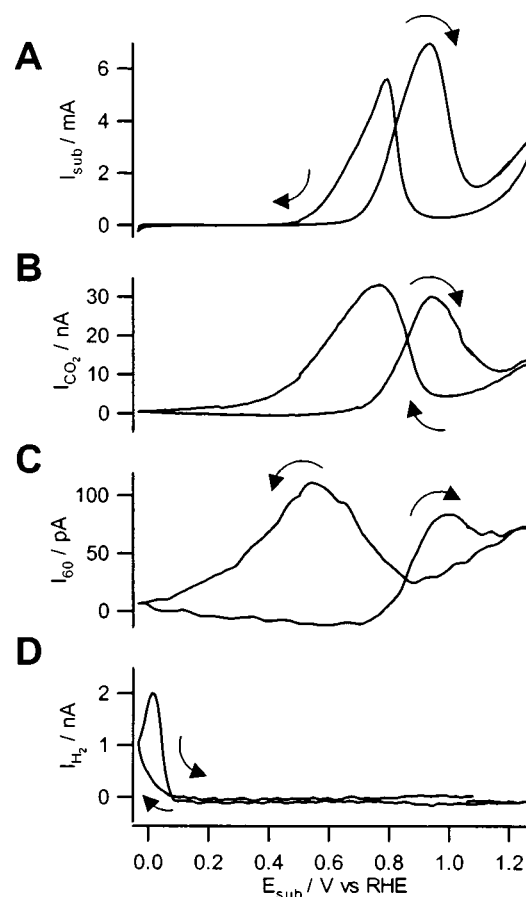


Figure 6. Electrochemical and mass spectrometric response of Pt substrate during methanol oxidation in a solution containing 1.0 M CH₃OH, 0.5 M H₂SO₄ at a scan rate of 10 mV s⁻¹. (A) Electrochemical current, (B) CO₂ ion current ($I_{\text{CO}_2}, m/z = 44$), (C) methyl formate ion current ($I_{60}, m/z = 60$) and (D) hydrogen ion current ($I_{\text{H}_2}, m/z = 2$). Arrows indicate direction of potential scan. The ion currents are adjusted by 9, 15, and 3 s for the signals in B, C, and D to compensate for the associated measurement delay times.

scanned in the positive direction. As the potential reaches ~0.7 V, anodic current increases due to methanol oxidation. Methanol oxidation presumably commences in concert with the formation of Pt hydroxides, which serve to remove the surface-bound decomposition products. The methanol oxidation current peaks at 0.8 V and then drops due to formation of a Pt oxide layer. Methanol oxidation on the Pt oxide surface occurs at potentials in excess of 1.0 V. During the reverse scan, a current peak is observed at 0.7 V corresponding to methanol oxidation on clean Pt. This current subsequently decreases as methanol decomposition products adsorb and deactivate the surface.

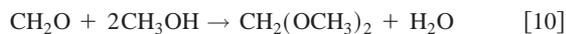
Simultaneous measurement of mass spectrometer ion currents during methanol oxidation can be used to further characterize this reaction. Figure 6B depicts the ion current for CO₂ ($m/z = 44$). A comparison of the ion-current signal for CO₂ with the electrochemical current indicates that they change in a similar fashion. An increase in electrochemical current results in an increase in CO₂ ion current. This reflects a CO₂ evolution rate that is proportional to the methanol oxidation current. A few subtle differences are noted, however. The maximum electrochemical current is observed during oxidation on Pt metal at 0.8 V during the positive potential scan while the largest CO₂ signal is observed during the negative potential scan at 0.7 V. This would suggest that a greater current efficiency, which corresponds to a greater conversion of methanol to carbon monoxide, occurs on the bare Pt metal during the negative potential scan. The negative potential scan provides a “fresh” platinum surface by

reduction of Pt oxides while the positive scan corresponds to a surface that has been covered with methanol decomposition products.

One particular advantage of using DEMS to characterize electro-oxidation reactions is the ability to detect partial oxidation products in addition to the complete oxidation product carbon dioxide.⁴⁰ The two primary partial oxidation products of methanol oxidation are formaldehyde and formic acid. Both species represent undesirable products and the source of losses in current efficiency. Formaldehyde can be formed by a two-electron oxidation of methanol while formic acid forms by a four-electron oxidation. However, formaldehyde and formic acid are difficult to detect directly by mass spectrometry in a methanol-containing solution due to m/z overlap and low volatility.⁴⁰ A solution to this dilemma for formic acid is the ability to detect it indirectly via methyl formate. Although methyl formate is not itself a direct partial oxidation product of methanol oxidation, it is created by the reaction of formic acid and methanol in the electrolyte solution



This reaction is quite fast in the presence of high methanol concentration and allows the ion current for methyl formate at $m/z = 60$ to be used to deduce formic acid concentration. In principle, a similar indirect detection is possible for formaldehyde through its reaction with methanol to produce dimethoxymethane ($m/z = 75$).

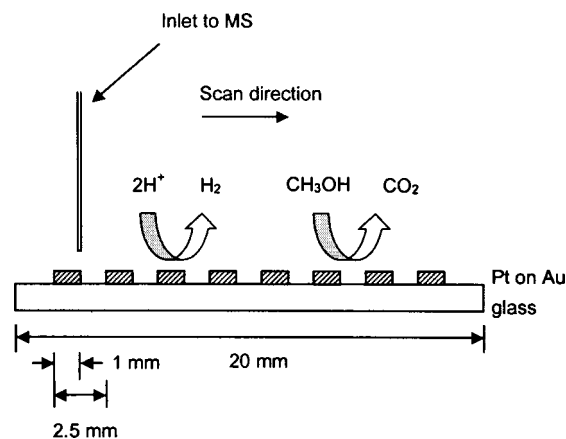


However, this product has only been detected in DEMS studies at high temperatures.⁶⁰ Nevertheless, the formation of significant formaldehyde near ambient conditions has been demonstrated using fluorescence detection.⁶¹

The ion current for methyl formate ($m/z = 60$) follows a trend that is similar to CO_2 . Peaks in the methyl formate signal are observed associated with peaks in the electrochemical current. The methyl formate peaks tend to trail the electrochemical peaks due to the lower diffusion coefficient of this species. Nevertheless, the observation of methyl formate in parallel with both electrochemical current and CO_2 production clearly indicates the evolution of formic acid during methanol oxidation. Notably, formic acid is thought to be a species in the parallel reaction pathway for methanol and its detection here and in prior DEMS studies confirms this path.^{40,44} As with the CO_2 signal, the methyl formate signal exhibits a maximum for methanol oxidation on clean Pt during the negative potential scan.

The signal corresponding to hydrogen ($m/z = 2$) is also measured during these experiments (Fig. 6D). Hydrogen is not expected to be evolved during methanol oxidation. However, during negative excursions in the electrode potential, hydrogen is detected as a result of the HER. The observation of hydrogen evolution indicates that this reaction proceeds through a partially deactivated surface. The Pt substrate is coated with sufficient methanol decomposition products to suppress hydrogen adsorption as seen in the substrate current (Fig. 6A).

Surface imaging and catalyst screening.—One of the benefits of the SDEMS configuration over traditional DEMS is that the detector inlet consists of a small diameter capillary tube that can locally sample the solution environment near an electrode surface. When coupled to a high resolution positioning system, this provides spatial mapping capabilities. This capability was demonstrated here using a band electrode assembly. Scheme 2 depicts the substrate construction and capillary inlet position used for imaging studies. The substrate comprised a series of band electrodes of 1 mm width and 2.5 mm period. The bands comprised vapor deposited gold on glass with a layer of electrodeposited platinum at the outer surface. The substrate was placed in a solution containing 1.0 M CH_3OH and 0.5 M H_2SO_4 in order to sample, in sequential measurements, the products of methanol oxidation and hydrogen evolution. During these experiments, the Pt bands were shorted to each other and held at the same potential. For hydrogen evolution, the electrode potential was held



Scheme 2. Schematic of electrodeposited Pt-on-Au band electrodes and capillary inlet tip to mass spectrometer during mapping experiments.

at -0.05 V (vs. RHE) to reduce protons in the solution to H_2 . For methanol oxidation the substrate was held at 0.7 V to oxidize CH_3OH to CO_2 . The capillary inlet was positioned at a separation of about $100 \mu\text{m}$ from the substrate and rastered perpendicular to the band axis at a scan rate of $25 \mu\text{m/s}$. In the methanol oxidation experiments, the electrode potential was held for 15 min before imaging in order to approach a steady oxidation current at the various electrodes.

Figure 7 shows the ion currents corresponding to H_2 and CO_2 as a function of position on the substrate. The H_2 signal depicts the variation in ion current as a function of spatial position as the substrate bands are reducing protons to hydrogen at a potential of -0.5 V. An increase in ion current at $m/z = 2$ is observed as the inlet is scanned over each band. A minimum in current is observed between the bands. Notably, the CO_2 ion current during this measurement was unchanged as a function of position (not shown). The maximum and minimum H_2 signals are approximately constant at and between each band, which is expected as the bands are all the same size and Pt content. A similar behavior was found for the variation in CO_2 ion current during methanol oxidation. The CO_2 signal varied be-

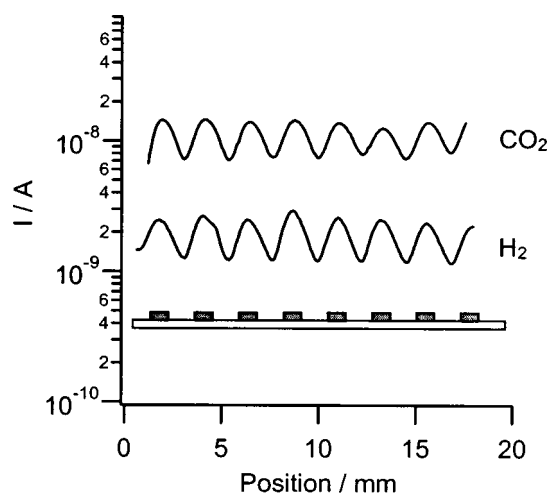
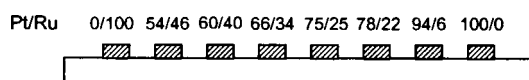


Figure 7. Ion currents for hydrogen ($I_{\text{H}_2}, m/z = 2$) and CO_2 ($I_{\text{CO}_2}, m/z = 44$) as a function of spatial position for a capillary separation of approximately $100 \mu\text{m}$ and a raster rate of $25 \mu\text{m s}^{-1}$. For hydrogen evolution, the substrate was held at a constant potential of -0.05 V (vs. RHE). For methanol oxidation, the substrate was held at a constant potential of 0.5 V (vs. RHE) for 15 min before imaging with the SDEMS tip. Both measurements were performed in a solution containing 1 M CH_3OH and 0.5 M H_2SO_4 .



Scheme 3. Schematic of electrodeposited PtRu-on-Au band electrodes. The compositions for the electrodes are given in percentages as determined by Auger electron spectroscopy.

tween nearly constant high and low values on top and between the Pt bands while held at a potential of 0.7 V, corresponding to methanol oxidation. The hydrogen ion current was unchanged as a function of position during this latter measurement.

Clearly, the spatial resolution of the SDEMS tip is poorer than that found with other scanning probe techniques such as the atomic force or scanning electrochemical microscopes. This is expected as the capillary inlet in this system had a diam of 150 μm , and could not resolve features below this size. Smaller capillary inlets can be used to improve imaging resolution. However, this will be achieved at the expense of detection of the mass signals as a necessarily smaller flux of gas will enter the ionization chamber with a smaller inlet diameter. Thus, there is a trade-off between image resolution and ion signal in this technique. In addition, the large o.d. of the capillary tube at 1.5 mm used in these studies prevented very small tip/sample separations, which also limits the spatial resolution. The outer capillary diameter may also present a mass transfer problem when studying reactions at lower concentrations where diffusion within the capillary/substrate gap is limited. These issues are currently being addressed by reducing the capillary o.d. and also via forced convection to the capillary inlet.

An inherent advantage of the SDEMS imaging system for combinatorial studies is that it can quantitatively detect a number of chemical species in liquid environments. In particular, as was demonstrated in Fig. 6, SDEMS was able to detect some of the partial and complete oxidation products of interest to anode reactions in low temperature fuel cells. The ability of SDEMS to function as a screening tool for methanol oxidation was demonstrated here by measuring the evolution of CO_2 and methyl formate on a series of electrodeposited Pt-Ru electrodes. Scheme 3 depicts the test sample used in this example. The substrate consists of the gold-on-glass band electrodes as depicted in Scheme 2, but with a range of Pt-Ru electrodeposits on the electrode surfaces. The compositions of these electrodes range from pure Pt to pure Ru that were created by pulsed electrochemical deposition from solutions containing H_2PtCl_6 and RuCl_3 at various concentration ratios (*vide supra*). The compositions of these electrodes as listed in Scheme 3 were determined with AES. Details of these electrodes and further electrochemical and mass spectrometry studies will be presented in a subsequent publication.

SDEMS scans over the electrodeposited Pt_xRu_y band electrodes are shown in Fig. 8. In these measurements, all 8 bands were electrically shorted and placed in a 1.0 M methanol and 0.5 M H_2SO_4 solution. The MS capillary inlet was placed in close proximity to the substrate at a separation of approximately 100 μm . The bands were then held at different potentials for a period of 15 min before the capillary was scanned over the bands at a rate of 25 $\mu\text{m s}^{-1}$. The ion currents corresponding to CO_2 ($m/z = 44$) and methyl formate, HCOOCH_3 ($m/z = 60$) were monitored as a function of position on the substrate. Figure 8A shows the CO_2 ion currents as a function of position and potential. In these results, the left most band contains 100% Ru and the right most band contains 100% Pt with the bands in between containing varying compositions of Pt and Ru. At potentials below 0.4 V, no CO_2 was detected. However, at 0.40 V, a broad CO_2 signal was detected over the bands containing between 6 and 40% Ru. This suggests that methanol oxidation had begun at these electrodes. With increasingly positive potentials, the broad CO_2 signal increased and features associated with individual electrodes emerged. At 0.55 V and above, distinct CO_2 evolution from the bands containing 34, 25, 22, and 6% Ru was indicated. At 0.65 V,

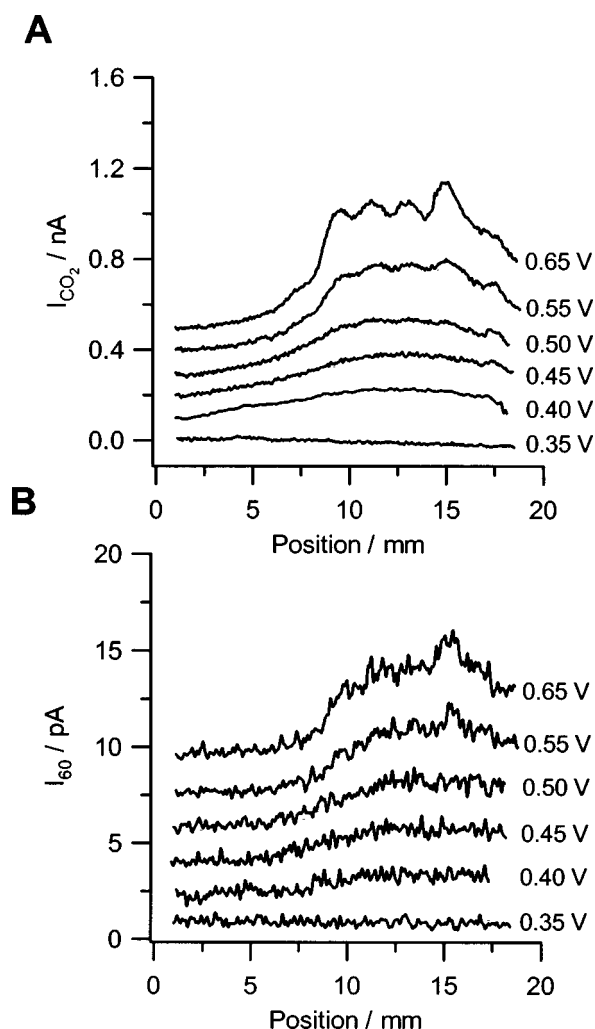


Figure 8. Ion currents detected for (A) CO_2 ($I_{\text{CO}_2}, m/z = 44$), and (B) methyl formate ($I_{60}, m/z = 60$) during methanol oxidation at electrodeposited Pt_xRu_y samples as a function of applied substrate potential in a solution containing 1 M CH_3OH and 0.5 M H_2SO_4 . Schemes 2 and 3 depict the band electrode structure and compositions. The electrode potentials were held for 15 min to obtain a constant current value before imaging.

the band containing 6% Ru gave the highest CO_2 current, suggesting that it had the highest activity under those conditions.

Simultaneous detection of methyl formate (Fig. 8B) evolution at the Pt_xRu_y band electrodes indicates a similar trend. Methyl formate is not observed at potentials below 0.4 V. At 0.4 V, a broad signal is detected at $m/z = 60$ over the bands containing less than 40% Ru. The magnitude of the methyl formate current also increased as the electrode potential increased. The magnitude of the methyl formate current at the various electrodes mimicked that of the CO_2 signal. The 6% Ru band gave the highest methyl formate current at 0.65 V. Notably, these results are consistent with measurements in which the SDEMS tip was held stationary over each electrode while the electrode potential was scanned or stepped to various potentials. A more detailed analysis of these results is the subject of a subsequent publication.

Conclusions

This manuscript demonstrates a new imaging tool, SDEMS. This technique is based upon the original design of the DEMS but with a modified inlet in the form of a membrane-coated capillary and 3-D positioning system that provides surface imaging capabilities. This technique can be applied to a range of problems of importance to

fuel cell catalysis and provides quantitative information about the evolution of partial and complete oxidation products. In addition, the ability to measure species in solution near an electrode surface at specific spatial locations has additional analytical capabilities of particular relevance for combinatorial studies. In this work, we have demonstrated the ability of SDEMS to be used as a screening tool to detect carbon dioxide and methyl formate evolution during methanol oxidation at a series of Pt_xRu_y electrodes. We are currently extending these studies to characterize a range of catalyst systems in array and gradient form with a diverse set of anode fuels.

Acknowledgments

The authors would like to acknowledge the Office of Naval Research for a Young Investigator Award, the National Science Foundation for a CAREER Award, the Camille and Henry Dreyfus Foundation for a New Faculty Award, and the Donors of The Petroleum Research Fund as administered by the American Chemical Society, for partial support of this research.

The University of Virginia assisted in meeting the publication costs of this article.

References

- P. N. Ross, in *Electrocatalysts*, P. N. Ross and J. Lipkowski, Editors, p. 1, Wiley, New York (1998).
- A. J. Appleby and F. R. Foulkes, *Fuel Cell Handbook*, Van Nostrand Reinhold, New York (1989).
- J. Larminie and A. Dicks, *Fuel Cell Systems Explained*, John Wiley & Sons, Ltd., New York (2000).
- H. Kita, H. Naohara, T. Nakato, S. Taguchi, and A. Aramata, *J. Electroanal. Chem.*, **386**, 197 (1995).
- N. M. Marković, B. N. Grgur, C. A. Lucas, and P. N. Ross, *J. Phys. Chem. B*, **103**, 487 (1999).
- M. Watanabe, M. Uchida, and S. Motoo, *J. Electroanal. Chem. Interfacial Electrochem.*, **229**, 395 (1987).
- H.-F. Oetjen, V. M. Schmidt, U. Stimming, and F. Trila, *J. Electrochem. Soc.*, **143**, 3838 (1996).
- Y. Y. Tong, H. S. Kim, P. K. Babu, P. Waszczuk, A. Wieckowski, and E. Oldfield, *J. Am. Chem. Soc.*, **124**, 468 (2002).
- C. Roth, N. Martz, F. Hahn, J.-M. Léger, C. Lamy, and H. Fuess, *J. Electrochem. Soc.*, **149**, E433 (2002).
- H. A. Gasteiger, N. M. Markovic, and P. N. Ross, *J. Phys. Chem.*, **99**, 8945 (1995).
- Y. Morimoto and E. B. Yeager, *J. Electroanal. Chem.*, **444**, 95 (1998).
- B. N. Grgur, N. M. Markovic, and P. N. Ross, *J. Phys. Chem. B*, **102**, 2494 (1998).
- B. N. Grgur, G. Zhuang, N. M. Markovic, and P. N. Ross, *J. Phys. Chem. B*, **101**, 3910 (1997).
- H. Nakajima and H. Kita, *Electrochim. Acta*, **35**, 849 (1990).
- B. Gurau, R. Viswanathan, R. Liu, T. S. Lafrenz, K. L. Ley, E. S. Smotkin, E. Reddington, A. Sapienza, B. C. Chan, T. E. Mallouk, and S. Sarangapani, *J. Phys. Chem. B*, **102**, 9997 (1998).
- Z. Jusys, T. J. Schmidt, L. Dubau, K. Lasch, L. Jörissen, J. Garche, and R. J. Behm, *J. Power Sources*, **105**, 297 (2002).
- A. Lima, C. Coutanceau, J. M. Leger, and C. Lamy, *J. Appl. Electrochem.*, **31**, 379 (2001).
- W. F. Maier, *Angew. Chem. Int. Ed. Engl.*, **38**, 1216 (1999).
- B. Jandeleit, D. J. Schaefer, T. S. Powers, H. W. Turner, and W. H. Weinberg, *Angew. Chem. Int. Ed. Engl.*, **38**, 2495 (1999).
- E. Reddington, A. Sapienza, B. Gurau, R. Viswanathan, S. Sarangapani, E. S. Smotkin, and T. E. Mallouk, *Science*, **280**, 1735 (1998).
- T. Bein, *Angew. Chem. Int. Ed. Engl.*, **38**, 323 (1999).
- P. Claus, D. Honicke, and T. Zech, *Catal. Today*, **67**, 319 (2001).
- C. M. Snively, G. Oskarsdottir, and J. Lauterbach, *Catal. Today*, **67**, 357 (2001).
- A. Holzwarth, H.-W. Schmidt, and W. F. Maier, *Angew. Chem. Int. Ed. Engl.*, **37**, 2644 (1998).
- P. Cong, R. D. Doolen, Q. Fan, D. M. Giaquinta, S. Guan, E. W. McFarland, D. M. Poojary, K. Self, H. W. Turner, and W. H. Weinberg, *Angew. Chem. Int. Ed. Engl.*, **38**, 484 (1999).
- S. Senkan, K. Krantz, S. Ozturk, V. Zengin, and I. Onal, *Angew. Chem. Int. Ed. Engl.*, **38**, 2794 (1999).
- A. Nayar, R. Liu, R. J. Allen, M. J. McCall, R. R. Willis, and E. S. Smotkin, *Anal. Chem.*, **74**, 1933 (2002).
- M. G. Sullivan, H. Utomo, P. J. Fagan, and M. D. Ward, *Anal. Chem.*, **71**, 4369 (1999).
- S. Jayaraman and A. C. Hillier, *Langmuir*, **17**, 7857 (2001).
- B. C. Shah and A. C. Hillier, *J. Electrochem. Soc.*, **147**, 3043 (2000).
- Y. Gao, H. Tsuji, H. Hattori, and H. Kita, *J. Electroanal. Chem.*, **372**, 195 (1994).
- A. D. Modestov, S. Srebnik, O. Lev, and J. Gun, *Anal. Chem.*, **73**, 4229 (2001).
- L. Grambow and S. Bruckenstein, *Electrochim. Acta*, **22**, 377 (1977).
- O. Wolter and J. Heitbaum, *Ber. Bunsenges. Phys. Chem.*, **88**, 2 (1984).
- V. M. Schmidt, R. Ianniello, E. Pastor, and S. Gonzalez, *J. Phys. Chem.*, **100**, 17901 (1996).
- W. Z. Lu, X. M. Xu, and R. B. Cole, *Anal. Chem.*, **69**, 2478 (1997).
- Z. Jusys, H. Massong, and H. Baltruschat, *J. Electrochem. Soc.*, **146**, 1093 (1999).
- R. Ianniello and V. M. Schmidt, *Ber. Bunsenges. Phys. Chem.*, **99**, 83 (1995).
- B. Bittins-Cattaneo, E. Cattaneo, P. Königshoven, and W. Vielstich, in *Electroanalytical Chemistry: A Series of Advances*, A. J. Bard, Editor, p. 180, Marcel Dekker, Inc., New York, (1991).
- H. Wang, T. Löffler, and H. Baltruschat, *J. Appl. Electrochem.*, **31**, 759 (2001).
- S. Wasmus and W. Vielstich, *Electrochim. Acta*, **38**, 185 (1993).
- N. Fujiwara, K. A. Friedrich, and U. Stimming, *J. Electroanal. Chem.*, **472**, 120 (1999).
- Z. Jusys and R. J. Behm, *J. Phys. Chem.*, **105**, 10874 (2001).
- Z. Jusys, J. Kaiser, and R. J. Behm, *Langmuir*, Submitted.
- J. Willsau, O. Wolter, and J. Heitbaum, *J. Electroanal. Chem. Interfacial Electrochem.*, **185**, 163 (1985).
- S. Wilhelm, W. Vielstich, H. W. Buschmann, and T. Iwasita, *J. Electroanal. Chem. Interfacial Electrochem.*, **229**, 377 (1987).
- T. Iwasita, W. Vielstich, and E. Santos, *J. Electroanal. Chem. Interfacial Electrochem.*, **229**, 367 (1987).
- J. L. Rodriguez and E. Pastor, *Electrochim. Acta*, **44**, 1173 (1998).
- W. Chrzanowski and A. Wieckowski, *Langmuir*, **13**, 5974 (1997).
- E. Herrero, J. M. Felio, and A. Wieckowski, *Langmuir*, **15**, 4944 (1999).
- S. R. Brankovic, J. X. Wang, Y. Zhu, R. Sabatini, J. McBreen, and R. R. Adžić, *J. Electroanal. Chem.*, **524**, 231 (2002).
- S. R. Brankovic, J. X. Wang, and R. R. Adžić, *Electrochem. Solid-State Lett.*, **4**, A217 (2001).
- E. L. Cussler, *Diffusion Mass Transfer in Fluid Systems*, Cambridge University Press, Cambridge, UK, (1997).
- B. A. Ogunnaike and H. W. Ray, *Process Dynamics, Modeling, and Control*, Oxford University Press, New York (1994).
- H. Baltruschat and U. Schmiemann, *Ber. Bunsenges. Phys. Chem.*, **97**, 452 (1993).
- I. Villegas and M. J. Weaver, *J. Chem. Phys.*, **101**, 1648 (1994).
- C. A. Lucas, N. M. Markovic, and P. N. Ross, *Surf. Sci.*, **425**, L381 (1999).
- V. S. Bagotzky and Y. B. Vassilyev, *Electrochim. Acta*, **12**, 1323 (1967).
- C. P. Wilde and M. Zhang, *Electrochim. Acta*, **39**, 347 (1994).
- S. Wasmus, J. T. Wang, and R. F. Savinell, *J. Electrochem. Soc.*, **142**, 3825 (1995).
- C. Korzeniewski and C. L. Childers, *J. Phys. Chem. B*, **102**, 489 (1998).